Supplementary Information

Long-wavelength infrared metamaterial absorber with polarization and angle insensitivity using compact hybrid cylinder structures

Wenqian Zhang,[a,b] Youxin Chen* [a,b] Jiang Wei[a,b],Yan Miao[a,b], Qingkang Wang[a] and Kaiyu Wu [a]

[a]National Key Laboratory of Advanced Micro and Nano Fabrication Technology, Shanghai Jiao Tong University, Shanghai, 200240, China
[b]Department of Micro/Nano Electronics, School of Electronic Information and Electrical Engineering, Shanghai Jiao Tong University, Shanghai, 200240, China

*Author to whom correspondence should be addressed: usingchen@sjtu.edu.cn

Contents

S1. Calculated absorption spectra versus different structural parameters

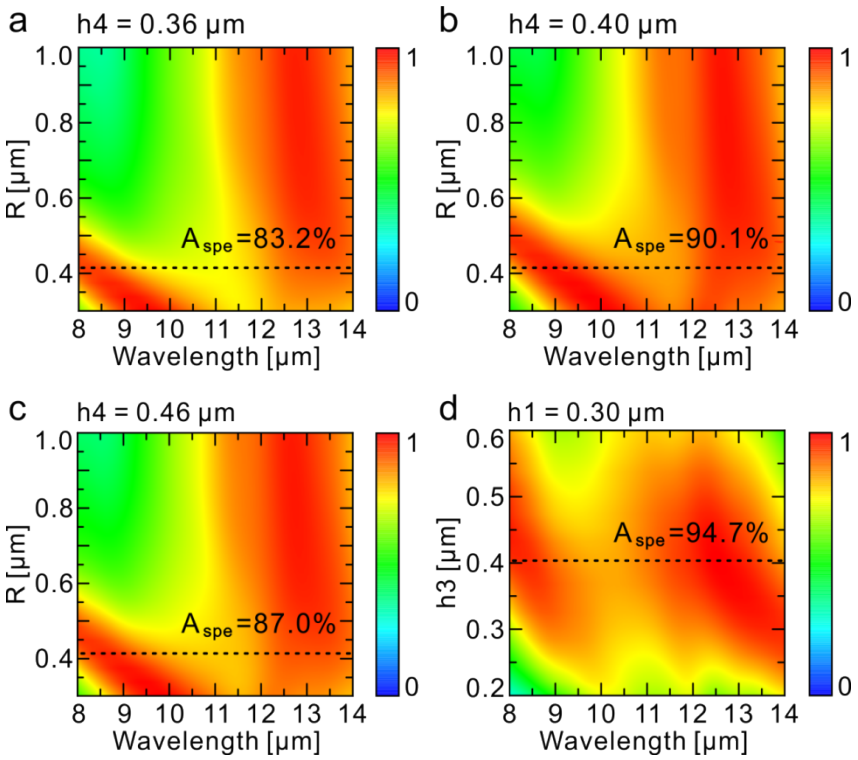

Fig. S1. Calculated absorption spectra over 8 to 14 μm versus different structural parameters. Unless otherwise noted, the default geometric parameters are: h_1 = 0.3 μm, h_2 = 0.02 μm, h_3 = 0.4 μm, h_4 = 0.4 μm, D = 0.84 μm, t_1 = 0.1 μm, and P = 1.27 μm.

The absorption performance of the HC-BMPA is theoretically optimized by first scanning D for three different h_4 values while keeping the other geometric parameters as default. Results are shown in **Figure S1(a-c)**. It can be found that when D = 0.82 μm and h_4 = 0.4 μm, A_{spe} reaches 90.1%. Then, choosing D = 0.82 μm and h_4 = 0.4 μm, h_1 and h_3 are scanned. Results are shown in **Figure S1(d).** A_{spe} reaches an extremum of 94.7% with the following structural parameters: h_1 = 0.3 μm, h_3 = 0.4 μm, h_4 = 0.4 μm, and D = 0.84 μm.

S2. Measured absorption spectrum of the Si wafer

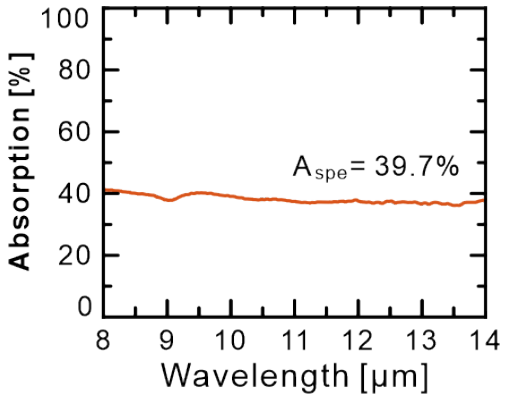

Fig. S2. Measured absorption spectrum of the Si wafer.

S3. Simulated electrical field distributions for the HC-BMPA versus incident angle

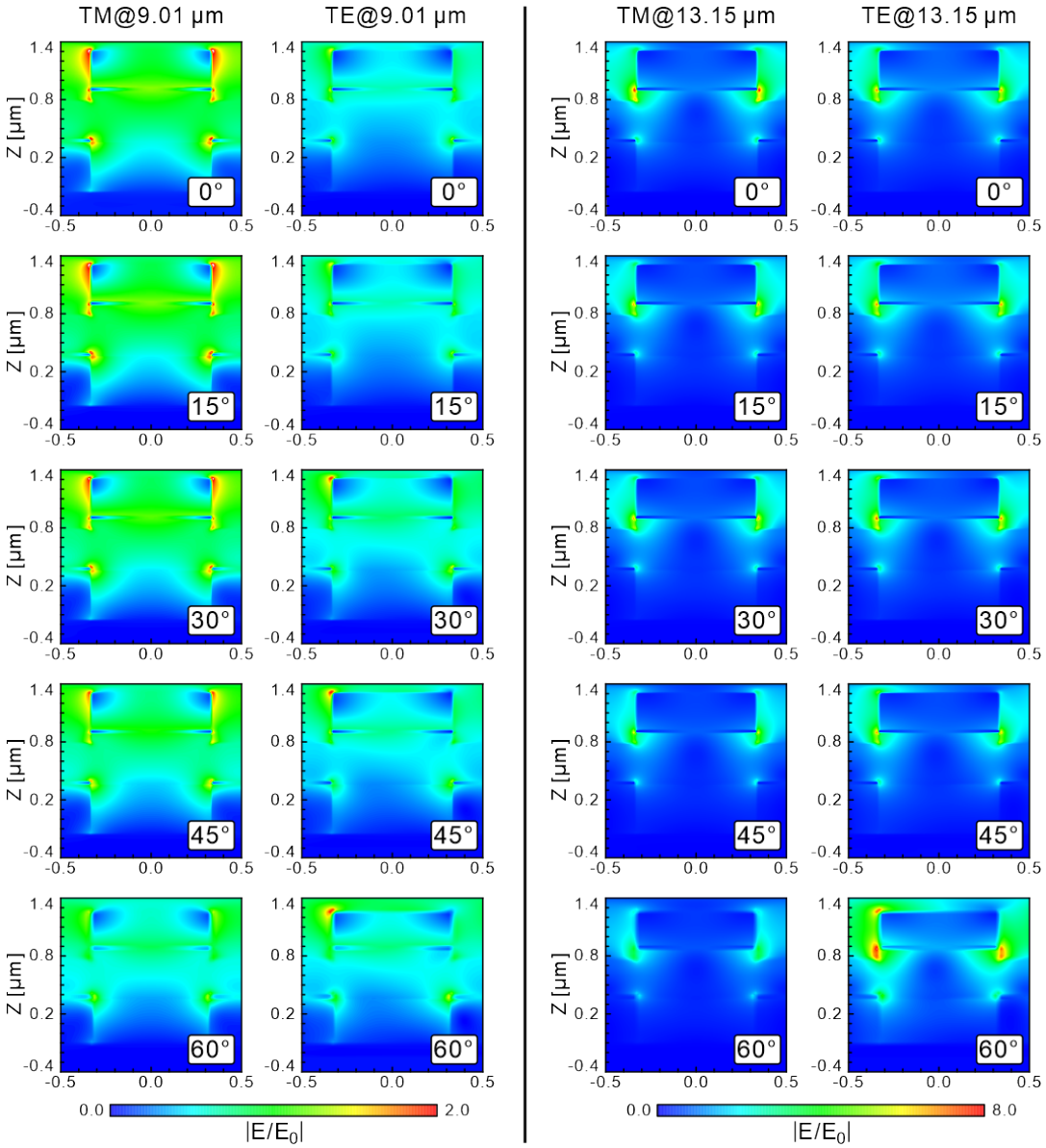

Fig S3. The simulated electrical field distributions $|E/E_0|$ at 9.01 μm and 13.15 μm under both TM and TE polarizations for the HC-BMPA versus incident angle.

It can be seen that with increased incident angle from 0° to 45°, the field distributions under TE polarization experience very slight change, while those under TM polarization vary significantly. This is because with increased incident angle, under TE polarization, the oscillation direction of the exciting electrical field remains the same, i.e., along the Y axis, while under TM polarization, it gradually changes from along the X axis towards along the Z axis. Therefore, the spectral averaged absorption Aspe is more insensitive under TE polarization comparing to TM polarization. Additionally, under TE polarization, when the incident angle further increases from 45° to 60°, the intensity of the localized electrical fields clearly becomes stronger. This should lead to increased Aspe, as is proved by Fig. 1h in the manuscript. The reason for this is because when the incident angle increases, the TE polarized excitation light interacts with more

structures.

S4. Thermal images of the HC-BMPA and a Si wafer under nature sunlight

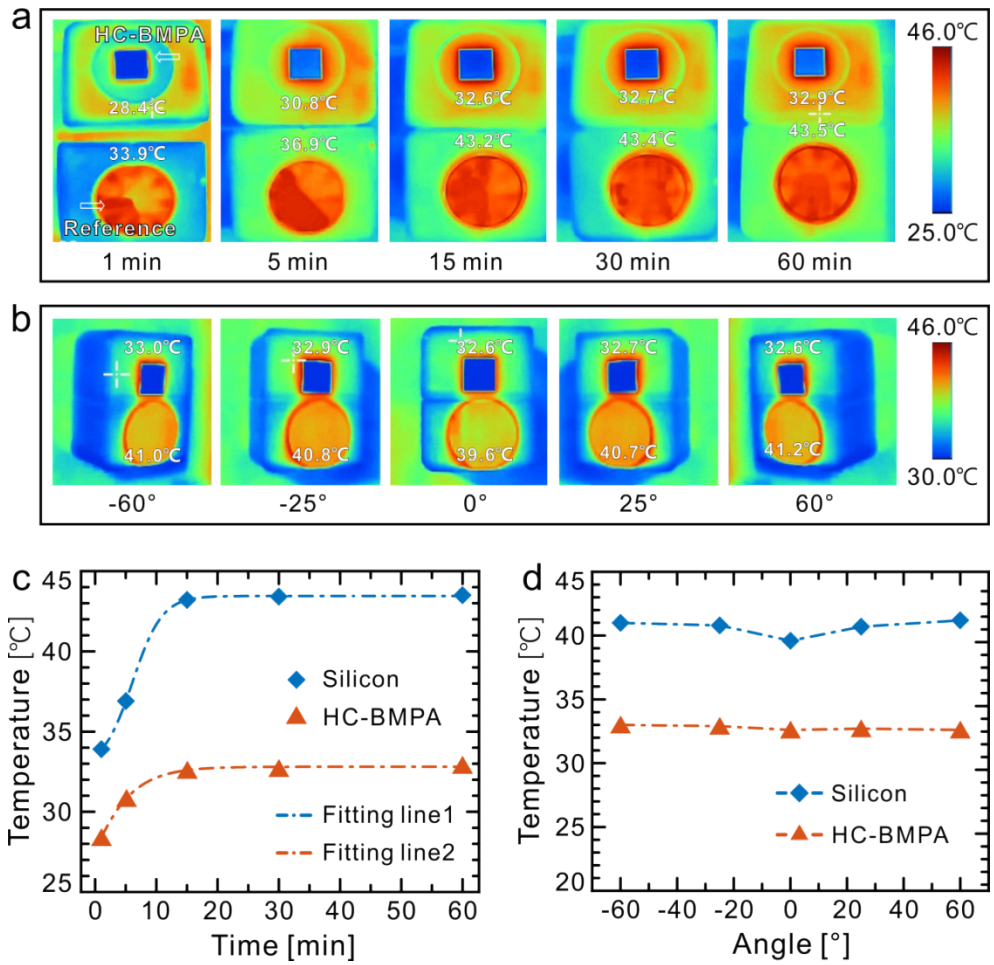

Fig. S4. Thermal images of the HC-BMPA and a referential Si wafer under nature sunlight (ambient temperature is 32℃). **(a)** under vertical radiation for different time, and **(b)** under different radiation angles near thermal equilibrium. **(c)** Temperature-time and **(d)** temperature-angle fittings corresponding to **(a)** and **(b)**, respectively.

Similar results are observed comparing to indoor tests. A HC-BMPA and a referential Si wafer are placed under nature sunlight (ambient temperature is 32℃, outdoor). The time-dependent thermal images are shown in **Fig. S2(a)**. Remarkable radiative cooling effects are observed. Near thermal equilibrium, i.e. after 60 min heating, the temperature of the HC-BMPA under nature sunlight is 32.9℃, which is 10.6℃ lower than that of the Si wafer (43.5℃). The corresponding temperature-time relation is plotted in **Fig. S2(c)**. The significantly lower heating rate and equilibrium temperature of the HC-BMPA demonstrate its outstanding outdoor cooling performance. **Fig. S2(b)** shows the outdoor infrared thermal images of the HC-BMPA and the Si wafer near thermal equilibrium under different radiation angles. The corresponding temperature-angle plot is shown in **Fig. S2(d)**. The temperature fluctuation is negligible for the HC-BMPA, thanks to its angle and polarization insensitive absorption characteristic. In summary, the presented HC-BMPA is promising in radiative cooling and related applications such as thermal emitter and imaging.

S5. Methods

Simulation: The Finite Difference Time Domain (FDTD) method was used to numerically analyze and optimize the metamaterial absorber shown in **Fig. 1** in the main text. A period of the structure is modelled. Periodic boundary conditions were used along the x and y directions, and perfectly matched layers (PML) were used in the z direction. The complex dielectric constants of Ti, Ge and SiO_2 were obtained by the Drude-Lorentz model. An adaptive mesh was employed.

Fabrication: The fabrication of the designed structure starts with a commercial 2-inch single-side polished silicon wafer purchased from Yuanjing electronic science and technology company. To clean the Si wafer, ultrasonic treatment was performed with acetone and NMP solutions for 5 min each. Then, the Si wafer was blow-dried by N_2 gas. Subsequently, a 0.1 μm bottom Ti film was sputtered onto the Si wafer by a Denton Multi-target Magnetic Control Sputtering System. A 0.4 μm thick SiO_2 film was deposited by an Oxford PECVD system (ICP180). Then, the SiO_2 film was patterned into SiO_2 disc array, through lithography and dry etching. A positive photoresist (AZ 5214E) was spin-coated on the SiO_2 film surface, at a rate of 4000 rpm, and baked at 110 °C for 50 s. After patterning by a stepper (NIKON-I12), the sample was developed with AZ 400 K developer. Dry etching employed a BOSCH process. The recipe was SF_6 based RIE at the etch step and C_4F_8 based deposition at the passivation step. The SiO_2 film was etched till the bottom Ti surface, and the remaining photoresist was removed by acetone. Then, the first Ge layer was deposited by an Oxford PECVD system (ICP180). Since the SiO_2 cylinders are produced by PECVD, the first Ge layer made by PECVD shall have better adhesion to SiO_2 comparing to those made by EBE or MS.[1] In addition, PECVD is a more isotropic process than EBE and MS,[2] so that the rendered Ge layer is more uniform on the sidewalls of the SiO_2 cylinders with a better step coverage. Moreover, the Ge layer deposited by PECVD has high blocking effect against moisture and alkaline ions. This would protect the first Ge layer from possible damage during subsequent processes.[2,3] Finally, Ti and Ge films were stepwise deposited by a Multi-target Magnetic Control Sputtering System for the MS-prepared sample, or by a Denton Electron Beam Evaporator for the EBE-prepared sample. Comparing to PECVD, physical vapor deposition methods such as EBE or MS do not involve chemical reactions, thus produce films with higher purity, better compactness, and smoother surface, beneficial for optical applications.[4-7]

Characterization: The morphological features of the HC-BMPAs were acquired using a high-resolution SEM (JSM-7800F, JEOL, Japan). The THERMO FISHER Infrared Spectrometer (Nicolet 6700, Spectral range 12000-350 cm^{-1}, SNR＞50000:1, Resolution＞0.09 cm^{-1}, Accuracy ＞0.01 cm^{-1}, America) was employed to measure the reflectance of samples. The measurements were referenced to a gold-coated flat silicon mirror. Thermal images were obtained by an IR camera (FOTRIC 285, FOTRIC, Infrared resolution 320×240, NETD ＜30 mk@30℃, Spectral response 7 – 14 μm, CN).

Reference

1 S A an, A. Dana and A. Aydinli, *J. Phys.: Condens. Matter.,* 2006, **15**, 185037.

2 S. A an, A. Celik-aktas, J. M. Zuo, A. Dana and A. Aydinli, *Appl. Phys. A.*, 2006, **83**, 1 07-110.

3 V. Y. Vasilyev, *2009 International Conference and Seminar on Micro/Nanotechnologies a nd Electron Devices*, 2009, pp. 104-111.

4 T. Lee, and S. Oh, *IEEE Trans. Electron Devices.,* 2024, 1–6.

5 S. Parola, E. Quesnel, V. Muffato, L. Guetaz, H. Szambolics, J. Bartringer, and A. Slaoui, *J. Nanopart. Res.,* 2012, **14**, 1085.

6 P. Basa, G. Molnár, L. Dobos, B. Pécz, L. Tóth, A.L. Tóth, A.A. Koós, L. Dózsa, Á. Nem csics, and Zs.J. Horváth, *J. Nanosci. Nanotechnol.*, 2008, **8**, 818–822.

7 K. Li, Y. Xiong, H. Wang, K. Zhang, L. Xu, X. Li, and H. Zhou, *Optoelectron. Lett.,* 2020, **16**, 298–302.